

Spectral shapes of the Lyman-alpha emission from galaxies: I. blueshifted emission and intrinsic invariance with redshift*

MATTHEW J. HAYES,¹ AXEL RUNNHOLM,¹ MAX GRONKE,² AND CLAUDIA SCARLATA³

¹*Stockholm University, Department of Astronomy and Oskar Klein Centre for Cosmoparticle Physics, AlbaNova University Centre, SE-10691, Stockholm, Sweden.*

²*Department of Physics & Astronomy, Johns Hopkins University, Baltimore, MD 21218, USA and Hubble fellow*

³*Minnesota Institute for Astrophysics, School of Physics and Astronomy, University of Minnesota, 316 Church Str. SE, Minneapolis, MN 55455, USA*

(Received June 3, 2020; Revised Sometime after that...; Accepted December 22, 2024)

Submitted to ApJ

ABSTRACT

We demonstrate the redshift-evolution of the spectral profile of H I Lyman-alpha ($\text{Ly}\alpha$) emission from star-forming galaxies. In this first study we pay special attention to the contribution of blueshifted emission. At redshift $z = 2.9\text{--}6.6$, we compile spectra of a sample of 229 $\text{Ly}\alpha$ -selected galaxies identified with the Multi-Unit Spectroscopic Explorer at the Very Large Telescope, while at low- z (< 0.44) we use a sample of 74 ultraviolet-selected galaxies observed with the Cosmic Origin Spectrograph onboard the Hubble Space Telescope. At low- z , where absorption from the intergalactic medium (IGM) is negligible, we show that the relative contribution of blueshifted emission (blue/red) increases rapidly with increasing equivalent width ($W_{\text{Ly}\alpha}$). This result does not, however, emerge at $z = 3\text{--}4$, and we use bootstrap simulations to demonstrate the blue emission to be suppressed by stochastic IGM absorption. Our main result is that the blue-peak contribution evolves rapidly downwards with increasing redshift: the blue/red flux ratio is $\approx 30\%$ at $z \approx 0$, but drops to 15% at $z \approx 3$, and to below 3% by $z \approx 6$. Applying further simulations of the IGM absorption to the unabsorbed COS spectrum, we demonstrate that this decrease in the blue-wing contribution can be entirely attributed to the thickening of intervening $\text{Ly}\alpha$ absorbing systems, with no need for additional H I opacity from local structure, companion galaxies, or cosmic infall. We discuss our results in light of the numerical radiative transfer simulations, the evolving total $\text{Ly}\alpha$ output of galaxies, and the utility of resolved $\text{Ly}\alpha$ spectra in the reionization epoch.

Keywords: radiative transfer – galaxies: evolution – galaxies: high-redshift – galaxies: intergalactic medium – galaxies: emission lines – galaxies: starburst

1. INTRODUCTION

The $\text{Ly}\alpha$ emission line, and its spectral profile, encode a wealth of information about both star-formation and various gas phases in galaxies, including the interstellar medium (ISM), the more tenuous circumgalactic

medium (CGM) and, at the highest redshifts, the intergalactic medium (IGM). Because of the abundance of atomic hydrogen and the nature of the H I atom, $\text{Ly}\alpha$ is intrinsically the brightest spectral feature of ionized nebulae, but also has the largest optical depth to absorption. $\text{Ly}\alpha$ is therefore sufficiently luminous to be observed from redshifts (z) out to above 9 (e.g. Hashimoto et al. 2018), but is then multiply scattered by H I atoms, and re-shaped by radiative transfer (RT) effects into which many galaxy properties enter (see Runnholm et al. 2020 for a thorough investigation, and Dijkstra 2014 and Hayes 2015 for reviews).

Corresponding author: Matthew J. Hayes
matthew@astro.su.se

* Based on observations made with the NASA/ESA Hubble Space Telescope, obtained from the data archive at the Space Telescope Science Institute. STScI is operated by the Association of Universities for Research in Astronomy, Inc. under NASA contract NAS 5-26555.

This absorption by H I may occur in both ‘conventional’ (=H I-dominated) atomic gas clouds or residual H I ions in H II-dominated gas. The Ly α RT, therefore, can be a problem covering various regions and physical scales. The emergent Ly α line profile will firstly be a reflection of the kinematics of the H II regions in which Ly α is intrinsically produced. However this velocity profile is subsequently modulated by scattering events within the H II region itself, that will introduce some degree of broadening depending upon the small scale gas densities. But Ly α photons may also have to traverse high column density, optically thick gas, that permits escape only after long excursions in frequency space (wing scatterings Adams 1972; Neufeld 1990). This generally high optical depth at line center introduces double-peaked profiles, consisting of blueshifted and redshifted components with little emission at line center ($\Delta v = 0$), and a separation that depends on the column density. Because gas is rarely static or homogeneous in the ISM, the density distribution, clumpiness, and dynamics of the neutral and dense ionized medium in galaxies will all influence the line profile. As starburst galaxies typically show moderate-velocity outflowing media (see reviews by Rupke 2018 and Veilleux et al. 2020 at low- z ; Erb 2015 at high- z) stronger redshifted Ly α peaks, with secondary weaker blue components, are commonplace.

Because the blue component of Ly α is easily suppressed by scattering in outflowing material, significant emission bluewards of the Ly α line center ($\Delta v < 0$) has become a key signpost of a low gas column density. Henry et al. (2015) first obtained UV spectra of a sample of ‘Green Pea’ galaxies: not only do these galaxies exhibit among the strongest Ly α lines known (average Ly α escape fraction of $\approx 25\%$ and EW of ≈ 60 Å), but a remarkable fraction of 9/10 also show double peaks. Similar results have since been presented in other low- z samples with similarly strong nebular EWs, and also high [O III]/[O II] ratios (Yang et al. 2017; Jaskot et al. 2017; Izotov et al. 2018, 2020). In Lyman break galaxies (LBG) at $z = 2 - 3$, the relative contribution of blueshifted Ly α also correlates strongly with the Ly α EW (Erb et al. 2014), and becomes even more prominent in very highly ionized galaxies (Erb et al. 2016; Trainor et al. 2016). These associations are also borne out by theoretical calculations and models. Verhamme et al. (2015) used Ly α radiation transfer simulations to show that a narrow velocity separation between two spectrally resolved peaks could be used as a signifier of column densities close to the limit of optical thickness at the Lyman edge; see Osterbrock (1962) and Hummer & Rybicki (1971) for the original discussions in the low optical depth limits. The implication that galax-

ies with narrow Ly α separations of below ≈ 250 km s $^{-1}$ would be LyC emitting galaxies was qualitatively borne out by recent observations (e.g. Izotov et al. 2018, see also Jaskot et al. 2019) and further theoretical work (e.g. Kimm et al. 2019; Kakiichi & Gronke 2019). As optical emission lines are hard to detect with high fidelity at $z \gtrsim 6$ because of redshifting to the IR, and absorption lines being equally hard because of the faint continuum, the Ly α spectral profile is a promising diagnostic for LyC emission at high- z .

Because Ly α is absorbed by H I, and the ionized fraction of the universe evolves with redshift, Ly α is a natural probe of the epoch of reionization (EoR; most recently reviewed by Dijkstra 2014). Studies began using first-order tests of the evolving Ly α luminosity function (LF; e.g. Kashikawa et al. 2006; Malhotra & Rhoads 2004, 2006) but, in light of the fact that galaxies may also assemble rapidly near the EoR, moved on to differential tests of Ly α evolution with respect to the underlying galaxy population. This has been cast as either the ‘volumetric’ Ly α escape fraction (Hayes et al. 2011; Dijkstra & Jeason-Daniel 2013; Konno et al. 2016; Wold et al. 2017) or as the fraction of strong LAEs among LBGs (Stark et al. 2010; Ono et al. 2012; Curtis-Lake et al. 2012; Schenker et al. 2012; Pentericci et al. 2014; De Barros et al. 2017; Mason et al. 2018; Kusakabe et al. 2020).

While the evolution of the average Ly α output may probe the neutral gas content of the universe at a certain redshift, re-ionization was also an inherently patchy processes because of the clustering of both cosmic gas and ionizing sources. Thus we need to ultimately progress beyond single averages at a given cosmic time (as in the studies above). Given that the EoR history and topology is a function of both structural overdensity (including gas/infall) and galaxy formation, it naturally follows that the blunt measure of neutral fraction vs time will vary with position (analogous to downsizing). Ultimately it must give way to a more nuanced approach, accounting for spatial/environmental, as well as temporal, variation. Ly α spectroscopy most likely offers the solution here, but in the form of a more detailed, spectrally resolved approach that targets the line profile.

To kick-start this science, a number of double-peaked Ly α emission lines have recently been identified at high- z . These include Aerith B at $z = 5.8$ (Bosman et al. 2019), NEPLA4 at $z = 6.5$ (Songaila et al. 2018) and COLA1 at $z = 6.6$ (Hu et al. 2016), which all show impressive Ly α double-peaks, strongly resemblant of the $z \approx 0$ compact starbursts (Henry et al. 2015; Jaskot et al. 2017; Izotov et al. 2020). According to simplified, homogeneous prescriptions for the neutral fraction

of the universe at these redshifts, these profiles should not exist, and even in modern radiation hydrodynamic simulations of the EoR, blue peaks at $z \gtrsim 6$ are rare (Gronke et al. 2020). Clearly the reionization progression is patchy, and Aerith B is a perfect example, being discovered inside the proximity zone of a luminous quasar. Bagley et al. (2017) recently calculated the bubble sizes necessary to explain the existence of two very luminous Ly α -emitter at $z \approx 6.4$, finding they must exist on Mpc scales. Matthee et al. (2018) performed a similar study using the spectral profile of COLA1 including its blue Ly α bump, and found comparable if somewhat smaller values; their calculation was revised upwards very recently by Mason & Gronke (2020) whose Bayesian inference places additional new constraints on the ionizing output and neutral fraction within the H II bubble, as well as the bubble radius itself.

The uncertainties and degeneracies in these approaches are significant, but will doubtless improve as more systems are discovered and data improve. While the universe beyond $z \approx 5$ is really the point of interest, these studies can be significantly informed by those from low- and mid- z . Specifically with regard to the Ly α profile analysis, it is never clear at high- z how much absorption can be attributed to the IGM, and how much is simply frequency redistribution in the ISM/CGM. Because galaxy populations evolve in many ways – mass, morphology, dust content, etc – we do not believe a priori that Ly α profiles from low- z should necessarily hold in a galaxy population that is 10 times younger/less evolved. However, it remains well-motivated to see how the high- z observables would look in the no-evolution case. We do not currently have the data to probe these effects deep into the EoR, but are able to test the null hypothesis (no evolution of the Ly α spectrum) out to z of almost 6 with existing large sample, which is exactly the contribution of this manuscript.

In this paper we study the evolution of the Ly α spectral line shape with redshift, and the impact of absorption from discrete H I-absorbing systems in the IGM. We use large samples of homogeneously-selected Ly α spectra that have recently become available: at high- z we adopt the MUSE-WIDE data (Urrutia et al. 2019; see also Herenz et al. 2017) in the CANDELS-Deep region of the GOODS-South field. These data provide spectra with resolving powers of $R(\equiv \lambda/\Delta\lambda) = 1800\text{-}3500$ over 44 arcmin², of 478 galaxies. For a baseline Ly α spectrum that is not attenuated by the IGM, we leverage various samples of low- z spectra observed with HST/COS. These observations are pointed at pre-selected galaxies, but have higher spectral resolving power ($R \approx 3000\text{-}$

22000) and are also obtained at redshifts where the IGM has little or no impact on the Ly α spectral profile.

We present an overview of the data, sample, and methods in Section 2, and Ly α -related measurements in Section 3. We describe the shapes of the ensemble Ly α profiles as a function of other key Ly α observables in Section 4. We present our results concerning redshift evolution in Section 5, where we mainly show that low- z spectral profiles, and a simply simulated IGM, can entirely reproduce the evolution of the Ly α spectral shape out to $z = 6$. In Section 6 we discuss these results in light of existing Ly α radiation transfer simulations and current knowledge of the IGM opacity. Section 7 presents some thoughts on the future application and limitations of our approach, and we present a final summary of our findings in Section 8. We adopt cosmological parameters of $\{H_0, \Omega_M, \Omega_\Lambda\} = \{70 \text{ km s}^{-1} \text{ Mpc}^{-1}, 0.3, 0.7\}$.

2. DATA AND METHODS

Here we describe the data upon which we draw and the methods used. These relate to the observational data themselves (2.1) our treatment of the IGM (2.2), and our estimation of systemic redshifts (z_{sys} ; 2.3). Details of the stacking procedure can be found where they are first applied, in Section 4.

2.1. Observational data

For this paper we draw upon a large compilation of data, for which the origin is described in detail in A. Runnholm et al (2020b, in preparation). Here we present only a brief overview.

2.1.1. HST/COS

HST/COS (Green et al. 2012) is an ultraviolet spectrograph onboard HST and in the settings we use provides moderate-resolution spectra with $R \approx 18000$ on average. It has a 2.5 entrance aperture, which naturally will sample a range of spatial scales, depending upon the redshift of the galaxy, which varies from object to object. Galaxies observed with HST/COS have all been pre-selected by the HST observers and identified as the best targets with a certain scientific objective in mind.

The COS data are drawn from the following general observer programs (with principal investigators in parentheses): GO 11522 (PI: Green), 11727 (Heckman), 12027 (Green), 12269 (Scarlata), 12583 (Hayes), 12928 (Henry), 13017 (Heckman), 13293 (Jaskot), 13744 (Thuan), 14080 (Jaskot), 14201 (Malhotra), 14635 (Izotov), 15136 (Izotov). Most of the spectra have been published in studies of galaxy winds and outflows, as well as their relation to Ly α output and kinematic properties (Heckman et al. 2011, 2015; Wofford et al. 2013; Rivera-Thorsen et al. 2015, 2017; Henry et al. 2015; Jaskot &

Oey 2014; Jaskot et al. 2017, 2019; Izotov et al. 2016, 2018; Yang et al. 2017, and more). It is beyond the scope of this paper to summarize the results of these studies but the selection identifies galaxies in the redshift range between $z = 0.020$ and $z = 0.44$, with a median value of $z = 0.177$. This places the Ly α emission line in either the G130M or G160M grating of COS, and delivers a spectral resolution between $R = 13000$ and 19000 depending upon lifetime position and redshift. We discard low-resolution spectra obtained with the G140L grating, which has also been obtained in some of the programs for a handful galaxies.

The large majority of the targets were selected by UV emission, usually from GALEX far-UV photometry but also slit-less spectroscopy of Ly α in the case of GO 12269. Most were also constrained in at least redshift by optical line emission, which almost exclusively comes from the Sloan Digital Sky Survey (SDSS). Further constraints may have been applied in terms of optical compactness, H α or [O III] equivalent widths, [O III]/[O II] ratios, and more. Attending mainly to the papers above, star formation rates (SFR) lie in the range from 0.1 to over $50 M_{\odot} \text{ yr}^{-1}$.

All spectra were obtained from the Mikulski Archive for Space Telescopes (MAST), and reduced homogeneously with the calibration pipeline (CALCOS), v.3.3.7. Systemic redshifts have been derived from simultaneously fitting up to 20 optical emission lines for sources with SDSS spectra, and from literature values (e.g. Cowie et al. 2011), otherwise. More details can be found in A. Runnholm et al (2020b, in prep). We continuum subtract each of the COS spectra by fitting low-order polynomial functions to the continuum, avoiding strong stellar and interstellar features, and firstly measure the Ly α flux. The COS sample was mostly UV-selected as discussed above, and the galaxies are not guaranteed have Ly α in emission; as Ly α emission is mandatory for this study we discard all galaxies with signal-to-noise ratio in Ly α less than 8. This leaves a sub-sample of 74 galaxies, for which the median Ly α luminosity is $1.25 \times 10^{42} \text{ erg s}^{-1}$.

2.1.2. VLT/MUSE

Unlike HST/COS, VLT/MUSE (Bacon et al. 2010, 2014) is a survey instrument. It is the first truly large-format integral field spectrograph, with a field-of-view of $60 \times 60 \text{ } \square''$. MUSE therefore delivers an emission line survey for Ly α -emitting galaxies between $z = 2.9$ and $z = 6.6$ with 100 % spectroscopic completeness. However the spectral resolution is somewhat lower than that of COS, and varies between $R = 1800$ at the blue end, and 3500 at the red end.

Many Ly α surveys have already been conducted with MUSE, but here we rely upon the MUSE-WIDE survey (Herenz et al. 2017; Urrutia et al. 2019). The main reason is that there are many pointings (44 fields), that are observed to a homogeneous depth (1-hour per pointing). Moreover the 1-dimensional data are easily accessible through the CDS/VisieR database.

MUSE-WIDE LAEs are continuum-subtracted by median filtering, and the exact techniques can be found in Runnholm et al (2020b, in prep). The Ly α luminosity is measured by numerical integration over a window that is 2500 km s^{-1} wide, and the errors are estimated by end-to-end Monte Carlo simulations. As with the COS spectra, we retain only spectra for which the SNR in Ly α exceeds 8. This leaves a sub-sample of 229 galaxies, for which the median Ly α luminosity is $3.1 \times 10^{42} \text{ erg s}^{-1}$.

We note that this Ly α selection at high- z , and UV selection at low- z , are very different strategies for identifying galaxies. This may introduce some bias, but is a necessary condition of contrasting low- z samples with large datasets at high- z with current facilities. We later perform an additional level of matching between the two samples; see Section 4.3 for more details.

2.2. Simulating the intergalactic medium absorption

We follow the method described in Inoue et al. (2014), which is based upon statistics of absorption line systems. The paper presents probability distribution functions for the column density of absorbing systems from the Ly α forest range up to damped Ly α absorbing systems, complete with their Doppler broadening distribution and redshift evolution. We implement the algorithms presented in Inoue et al. (2014) and calculate the total optical depth that ionizing radiation (LyC) experiences at a range of redshifts, where it is subject to direct absorption by photoionization, as well as exciting Lyman series transitions at lower redshift – we verify the performance of the code by testing against total optical depths published in the same paper.

The statistics of these absorbing populations and their evolution are both completely empirical and very well determined, and the great advantage of absorption selection is that it suffers no redshift bias. The numbers presented by Inoue et al. (2014) will represent a very realistic average absorption in a spatially uncorrelated universe. Note that this implies that the PDFs of the absorbers are treated as being spatially independent, and the approach does not account for spatial correlation of matter in the universe. Sightlines identified in observational campaigns, however, will by construction find regions that are on average over-dense compared to these IGM prescriptions (entirely randomized absorp-

tion). Several authors (Santos 2004; Dijkstra et al. 2007; Mesinger & Furlanetto 2008; Ilev et al. 2008; Laursen et al. 2011; Gronke et al. 2020) have discussed the effect of infall and structure local to galaxies, that will enhance the absorption of Ly α because of the increased neutral column crossing $\Delta z = 0$. Since the absorption line statistics are implemented randomly and drawn from Monte Carlo simulations, they provide a lower limit in comparison to absorption in the case of a structured universe. On the other hand, such simulations also neglect the local enhancement of the ionizing background that would be produced by both the observed galaxy and neighboring systems. These sources of ionizing radiation would act in the opposite direction and suppress the local absorption. While we acknowledge the possible discrepancy between the average cosmic absorption and the enhanced opacity that should occur close to galaxies, one of the key findings of this paper is that *there is no need for this additional absorption* (see Section 5.2).

2.3. Systemic redshift determination

We adopt a modified version of the z_{sys} estimation employed by the Lyman alpha Spectral Database (LASD¹; A. Runnholm et al. 2020b in preparation). The algorithm is not optimized to give a precise redshift on a case-by-case basis, but is designed to give a low dispersion for sample averages.

The algorithm requires an initial estimate for the redshift, for which we take the estimate from Urrutia et al. (2019). It then uses a decision tree and works on the heuristic that Ly α can be either single or double-peaked. The algorithm first calls a peak identifier to determine the number of peaks, which allows for N peaks, each of which must exceed SNR=5 and be recovered more than 95% of times in a 100-realization Monte Carlo simulation. In the case of doubly peaked Ly α the algorithm calculates the velocity of each peak and sets z_{sys} to the average value. In the case of a single peak it assumes the detected line corresponds to the redshifted main peak, and determines its maximum value. It then uses as ‘look ahead’ in the blueward wavelength direction until the flux density crosses zero; it records this velocity for each instance of the Monte Carlo simulation and assigns z_{sys} to the median value.

In Runnholm et al (2020b) we show this is accurate with a dispersion of 40 km s⁻¹ in a sample of low- z galaxies that have known z_{sys} – the same COS sample we use in this study that is presented in Section 2.1.1. In this study we apply an additional correction based upon

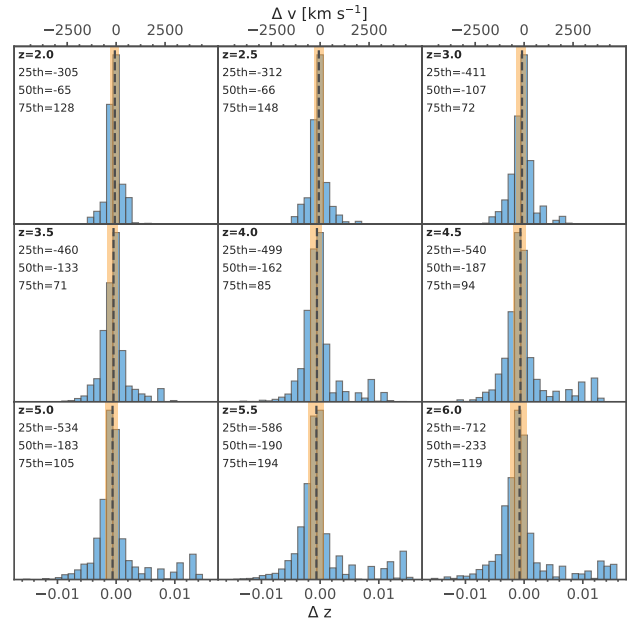


Figure 1. The performance of the systemic error estimation algorithm. The discrepancy for each object in the Monte Carlo simulation is given as Δz , which is defined as $z_{\text{LASD}} - z_{\text{sys}}$, where z_{sys} is derived from optical emission lines. The difference in velocities is given on the upper axis. The median value is shown with the dashed black line, and interquartile range in the orange region. Median and IQR ranges are also given as inset text, as velocities in km s⁻¹.

systematic offsets observed within the sample at higher redshifts. We adopt the same COS sample as previously described, and artificially redshift them to redshifts of 2.5 to 5.5 in steps of 0.5 redshifts. We then run a library of random IGM realizations at each of these redshifts using the method described in Section 2.2 and attenuate each of the redshifted spectra 50 times. We run the z -detection algorithm on each galaxy at each redshift, and examine the representative statistics of the output compared to the known z_{sys} . We show the results in Figure 1.

The algorithm recovers z_{sys} with a median offset of -65 km s⁻¹ at $z = 2$, which grows to -233 km s⁻¹ by $z = 6$. This is a result of two phenomena: firstly the blue peaks become systematically more suppressed with increasing redshift, because the IGM absorption preferentially removes weaker blue peaks. This causes the algorithm to more frequently switch from two-peak to one-peak mode as redshift increases. Moreover the thicker IGM as z approaches 6 starts to influence the red peak. Damping wings become visible in a minority of simulations, but the blue wing of the red peak becomes systematically more removed, shifting our z estimate to higher positive velocities.

¹ <http://lasd.lyman-alpha.com>

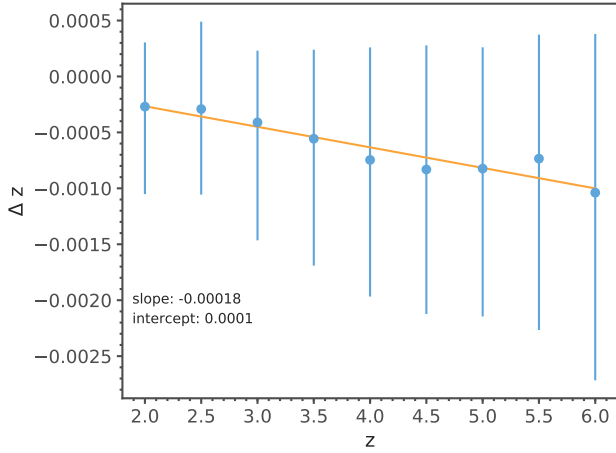


Figure 2. The performance of the z_{sys} identification with redshift. Redshift is shown on the abscissa, while Δz is shown on the ordinate-axis. Each point illustrates the median value from the simulated sample, and the error-bar shows the interquartile range. Our best fit is a linear function with the coefficients shown in the Figure.

This shift of the estimated z_{sys} with redshift is both expected and predictable, and we show the redshift evolution of Δz in Figure 2.

3. BASIC MEASUREMENTS AND SAMPLE CHARACTERIZATION

The measurements we make in this paper were all made using algorithms developed for the *Lyman alpha Spectral Database* (LASD; Runnholm et al 2020b) or from the measurements distributed and compiled by Urrutia et al. (2019). Here we present a brief overview. We also present a basic characterization in Section 3.2, and the first investigations of the line profile shapes can be found in in Section 4.

3.1. Measurements and quantities

The LASD measures 38 spectroscopic/kinematic properties of the $\text{Ly}\alpha$ spectra, most of which are fluxes/flux densities or velocities. In this study we also use $\text{Ly}\alpha$ luminosities derived from the LASD, which are computed by numerical integration over a spectral region 2500 km s^{-1} wide around $\text{Ly}\alpha$. This is done after continuum subtraction, and the continuum estimate is used to derive the equivalent width, $W_{\text{Ly}\alpha}$. We use these LASD-reported EWs for the COS sample. As $\text{Ly}\alpha$ is a resonance line it can be absorbed from the stellar continuum as well as produced in emission by nebulae/H II regions; in this study we define the $\text{Ly}\alpha$ flux as the total integral over the velocity range with no correction for blueshifted absorption. This is in part motivated by the fact that ostensibly pure emission lines can still be at-

tenuated to an unknown degree, and in part because the high- z galaxies are too faint to detect the continuum and the comparable correction could not be applied. More discussion on this is presented in Section 4.1.

As the MUSE-WIDE data are too shallow to detect the stellar continuum, the EWs report by the LASD are not robust. Instead we adopt the UV luminosities derived from HST broadband imaging. Each object in the Urrutia et al. (2019) data release contains an identifier to the HST-identified object in the catalog of Guo et al. (2013), which we then search for photometry in the five ACS bands, F435W, F606W, F775W, F814W, and F850LP. For the redshift of each galaxy, we first determine which is the bluest filter in the ACS set that has a central wavelength redwards of $\text{Ly}\alpha$, so that it samples more the stellar continuum than the IGM absorption. Then we calculate the contribution of the $\text{Ly}\alpha$ line (flux from Urrutia et al. 2019) to the broadband magnitude, allowing for both the filter width and relative throughput at the specific wavelength of $\text{Ly}\alpha$. We subtract this value from the broadband flux, and adopt the final line-subtracted magnitude for the galaxies' stellar continuum. In the stacking analyses we use the same algorithms to measure the blue/red flux ratio as in the individual cases.

3.2. Basic sample characterization

We present the $\text{Ly}\alpha$ luminosity and EW distributions of the two complete samples in Figure 3. The main panel shows the relation between the two quantities, while the vertical histogram above shows the distribution of $L_{\text{Ly}\alpha}$. The two horizontal histograms to the right show the total distribution of $W_{\text{Ly}\alpha}$ in the inner panel, while in the outer panel the COS sample has been restricted to $L_{\text{Ly}\alpha} \geq 10^{42} \text{ erg s}^{-1}$; this cut is designed to match the luminosities between the two samples, and is shown by the vertical dashed line in the main figure. The sample matching is discussed in more detail below and in Section 4.3.

The range of EWs overlaps well between the sample, spanning values above $\sim 200 \text{ \AA}$, even in the UV-selected low- z sample. The shapes of the EW distribution exhibit similar declines towards higher values, but different behavior in the lowest EW bins: being $\text{Ly}\alpha$ selected, the MUSE sample is under-represented at the lowest EWs (0–25 \AA) in this binning, while this is the most populated bin the UV-selected COS sample. The two samples are very different in $L_{\text{Ly}\alpha}$: both samples extend to a comparably high luminosity ($\approx 10^{43} \text{ erg s}^{-1}$), but the COS sample extends down to $L_{\text{Ly}\alpha} \approx 3 \times 10^{40} \text{ erg s}^{-1}$ while the MUSE data stop at $L_{\text{Ly}\alpha} = 10^{42} \text{ erg s}^{-1}$. In the high- z study that follows we remove low- z galaxies with

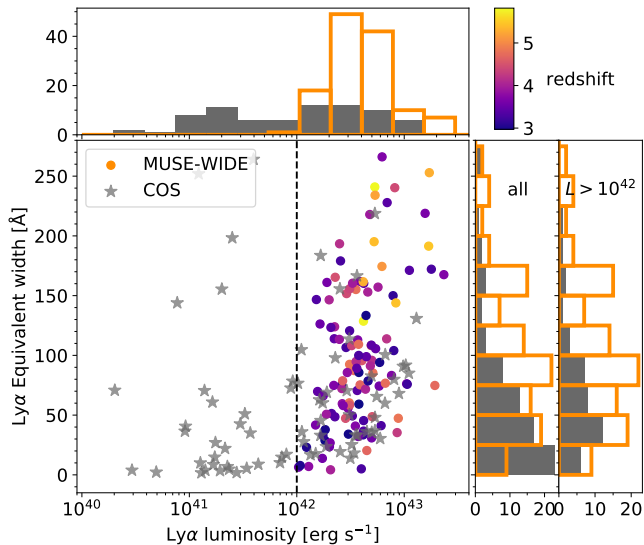


Figure 3. The range of $L_{\text{Ly}\alpha}$ and $W_{\text{Ly}\alpha}$ spanned by the COS sample (grey stars) and MUSE samples (colored circles). The MUSE data are color-coded by redshift, with the colorbar shown to the upper right. A histogram showing the $L_{\text{Ly}\alpha}$ distribution is shown above, and histograms showing $W_{\text{Ly}\alpha}$ are shown to the right: the first includes the total COS sample, while the second shows the COS sample after retaining only galaxies more luminous than the cutoff of $L_{\text{Ly}\alpha} > 10^{42} \text{ erg s}^{-1}$; this luminosity cutoff is illustrated by the dashed black line.

$L_{\text{Ly}\alpha} < 10^{42} \text{ erg s}^{-1}$, so as to match $L_{\text{Ly}\alpha}$ between the samples; this also has the effect of bringing the EW distribution more into agreement (right histogram). First, however, we perform a more general study of the line profiles in the stacked spectra to better understand the origin of the line profiles (blue bumps in particular) and include all COS galaxies so as to preserve the dynamic range in the sample.

4. LYMAN ALPHA PROFILES: RESULTS FROM STACKED SPECTRA

The bulk of the data analysis in this paper comes from differential comparison of stacked spectra. Because galaxies lie at different distances we perform the stacking on spectra shifted into the restframe: we divide $(1+z)$ out from the wavelength vectors, and multiply the same factor back in to the flux vectors (always units of $\text{erg s}^{-1} \text{ cm}^{-2} \text{ \AA}^{-1}$) so that the equivalent widths are preserved. We multiply all flux vectors by $4\pi d_L^2$ to obtain luminosity density vectors, with units $\text{erg s}^{-1} \text{ \AA}^{-1}$. Every spectrum is then resampled onto the same velocity grid and co-added: we always record both the mean and median spectrum.

4.1. *HST*/COS data at $z < 0.4$

We show the combined $\text{Ly}\alpha$ profiles of the COS sample in Figure 4, where we examine how the profile shape varies as a function of luminosity and EW. It comes as no surprise that when dividing out the sample by $L_{\text{Ly}\alpha}$, galaxies become more luminous (upper plots to the left of Figure 4). We note, however, that there appears to also be some evolution in the blue wing of the $\text{Ly}\alpha$ profile in that it appears to become disproportionately stronger in galaxies of higher $W_{\text{Ly}\alpha}$. This becomes much more obvious when the spectra are normalized by the maximum value of the red peak prior to coaddition: in the lower panels to the left of Figure 4 it is clear that as the luminosity decreases, so does the relative contribution of the blue bump, which drops systematically from the orange line (almost $10^{43} \text{ erg s}^{-1}$) to the purple line (100 times less luminous).

We suspect this first result comes from variations in the column of blueshifted absorbing material. There is no absorption from the intergalactic medium at this redshift, and outflows/galaxy winds result in a stronger absorption from interstellar material on the blue side of $\text{Ly}\alpha$. This becomes even more marked in the lowest EW bin, where the mean combination reveals true blueshifted absorption of the stellar continuum, and perhaps even a wing from damped absorption extending onto the red side of $\text{Ly}\alpha$ at a lower level. At intermediate luminosities, the wing contribution clearly increases from rough 10%, up to 20–30 % for the brightest galaxies.

We examine this trend further in Figure 5, where in grey we show how the blue/red flux fraction contrasts with $L_{\text{Ly}\alpha}$ and $W_{\text{Ly}\alpha}$ for the individual galaxies. Targeting positive blue-side emission only, we only include here galaxies for which the flux density bluewards of line center exceeds zero, and the majority of galaxies from the least luminous bin from Figure 4 are removed. $L_{\text{blue}}/L_{\text{red}}$ shows significant scatter at all luminosities and EWs. Overlaid in color we show the median values for each sub-sample, and encode the IQR as the error-bar. Attending to the left-most plot, $L_{\text{blue}}/L_{\text{red}}$ appears close to invariant of $L_{\text{Ly}\alpha}$ at the low $L_{\text{Ly}\alpha}$ end, but much of this effect comes from the removal of absorbing galaxies and pure P Cygni-like systems from the bins. In the last bin, however, $L_{\text{blue}}/L_{\text{red}}$ does jump by a factor of ≈ 2 to 0.34, but overall there is no correlation. However, a tight correlation is seen between $L_{\text{blue}}/L_{\text{red}}$ and $W_{\text{Ly}\alpha}$ (right figure), with Spearman’s $\rho = 0.60$, corresponding to $p = 7.5 \times 10^{-8}$ off 68 data-points. This result is highly significant, and indeed the points show that the lowest EW galaxies have $L_{\text{blue}}/L_{\text{red}}$ at the percent-level, which rises dramatically to $\approx 30\%$ at $W_{\text{Ly}\alpha}$ of $\approx 100 \text{ \AA}$. This result quantitatively echoes those demonstrated in

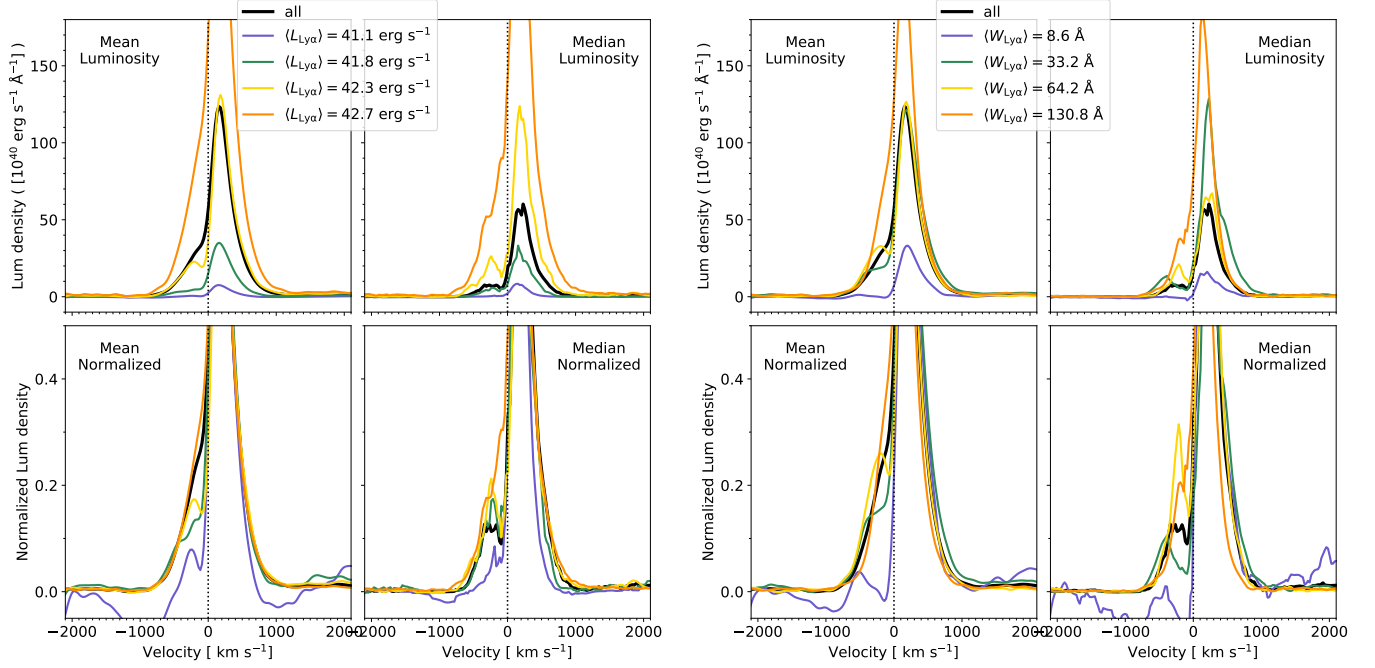


Figure 4. Each panel shows a stacked spectrum from the full sample of galaxies at $z < 0.4$ observed with HST/COS. We compare the spectral profiles as a function of $L_{\text{Ly}\alpha}$ (left 2×2 grid) and $W_{\text{Ly}\alpha}$ (right 2×2 grid). The sub-bins, divided by luminosity or EW are color coded with the values shown in the legend, while the total stack of the whole sample is shown in black. In each block of four panels, the left pair shows the mean combination and the right pair shows the median. Upper panels show the spectrum in absolute units of luminosity, while the lower panels show the spectra normalized by the maximum luminosity density, which is always that of the red peak. In the lower panels we zoom in on the luminosity axis so as to emphasize the blue wings.

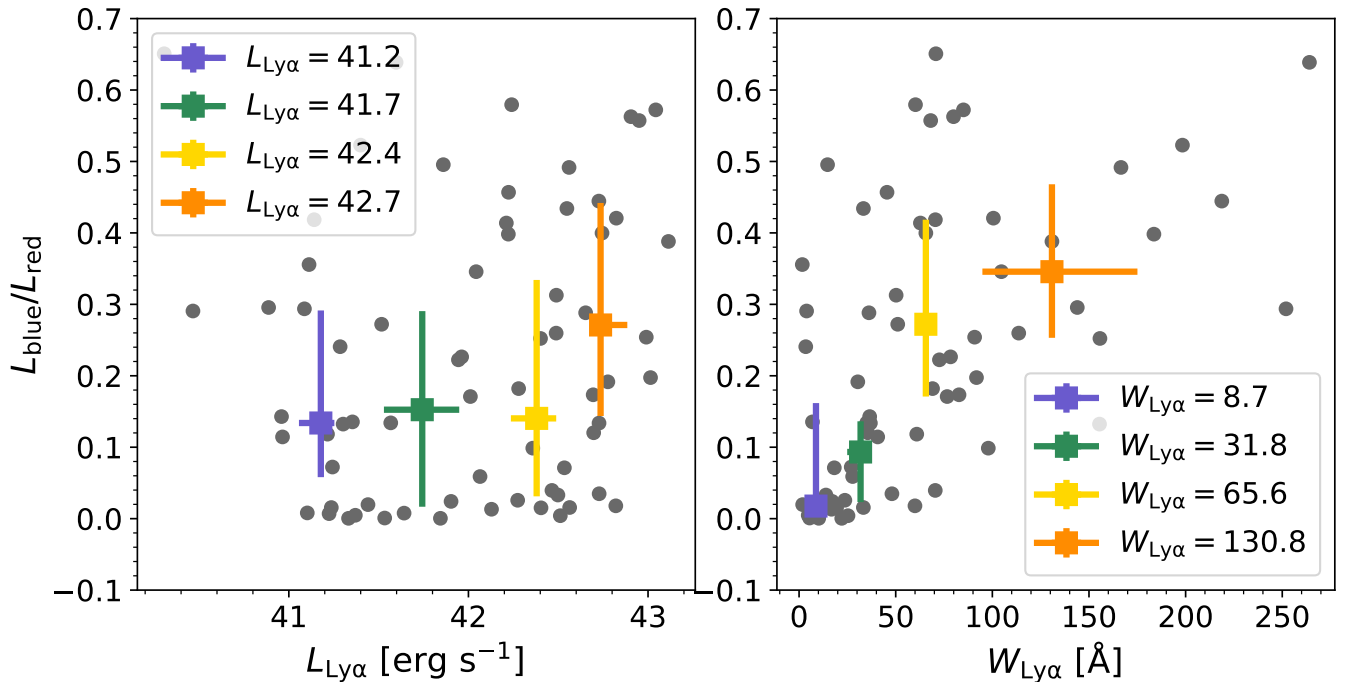


Figure 5. The relative contribution of the blue $\text{Ly}\alpha$ peak, expressed as the $L_{\text{blue}}/L_{\text{red}}$ ratio as a function of $L_{\text{Ly}\alpha}$ and $W_{\text{Ly}\alpha}$. It is similar to Figure 4 but on a galaxy-by-galaxy basis. The blue and red $\text{Ly}\alpha$ peaks are measured using the LASD software. Colored points are medians with interquartile ranges, and match with the bins in Figure 4.

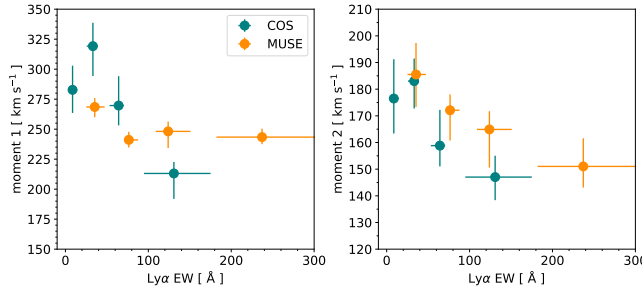


Figure 6. The evolution of the first and second moments of the red peak as a function of $W_{\text{Ly}\alpha}$. The complete range of luminosities of the COS sample are used and shown in green; the MUSE sample, which is more luminous but spans less dynamic range, is shown in orange. Median values and inter-quartile ranges are shown.

Henry et al. (2015) and Yang et al. (2017), whose $\text{Ly}\alpha$ EWs are among the highest observed and whose profiles also include the highest fraction of double peaks. Note, however, that the Henry et al. and Yang et al. observations are subsumed into our sample, and these results are not entirely independent.

We also note that galaxies with higher $W_{\text{Ly}\alpha}$ also show smaller systematic offsets in velocity (moment 1) and narrower red lines (moment 2), as shown in the normalized median profiles to the lower right left in Figure 4. The second moments of each bin decrease monotonically from 185 km s^{-1} at $W_{\text{Ly}\alpha} \approx 30 \text{ \AA}$ (shown by both MUSE and COS) to about 150 km s^{-1} at $W_{\text{Ly}\alpha} \approx 230 \text{ \AA}$ (probed only by MUSE), as shown in the right panel of Figure 6. We expect this is due to an effect of H I column density in which larger columns result in more $\text{Ly}\alpha$ scattering, which reduces the total emitted $W_{\text{Ly}\alpha}$ as the escape probability decreases. This additional scattering further results in broader $\text{Ly}\alpha$ lines that are systematically more redshifted.

4.2. VLT/MUSE data at $z > 2.9$

Figure 7 shows the stacked spectra obtained with VLT/MUSE. At these redshifts the IGM may have significant influence over the $\text{Ly}\alpha$ profile, especially in the blue side, so we temporarily restrict our analysis to $z < 4$ galaxies, so as to compromise between studying less absorbed galaxies while still maintaining a significant sample. Blue wings are also visible in the MUSE spectra, and examining all the lower panels of Figure 7 it is clear that some emission is visible to velocities as high as $\Delta v \approx -700 \text{ km s}^{-1}$. However unlike the lower- z COS spectra, this blue emission is visible in every bin of luminosity and EW. While the lines are not necessarily in agreement within the noise, relative intensity in the blue bumps does not show a serial decline as it does at lower- z : e.g. the green line clearly out-lies the others

in the EW comparison, but this is likely attributable to random processes.

In order to explore this lack of a trend further, we perform a bootstrap study using the low- z objects (no IGM absorption), and the IGM simulations described in Section 2.2. We first replace each galaxy in the $2.9 < z < 4$ MUSE sample with the low- z galaxy that has the closest $L_{\text{Ly}\alpha}$. We then randomly draw a sightline through the IGM to the MUSE redshift, attenuate the COS galaxy, and bin and stack this random sample. We examine the frequency with which a statistically significant ($p < 0.05$) trend is recovered. With samples the size of this MUSE subset ($N = 74$) the correlation is almost never reproduced: with just a few percent of realizations showing significant correlations. However when we artificially increase the bootstrap simulation to include ≈ 1000 objects (including galaxies more than once but with different random IGM sightlines) the trend does re-emerge, with the $L_{\text{blue}}/L_{\text{red}}$ ratio reduced by a factor of 2 compared to $z = 0$. This is exactly what would be expected for large samples, as the stochastic effect of the IGM is smoothed out over a large number of realizations.

In principle this method could be used to calculate the necessary sample size required in order to statistically study these trends at high-redshift, but many other factors will hold influence over the result. For example the precise recovery will also depend upon the signal-to-noise ratio of both the high- z data and the low- z data we use to simulate it, and the result will also be redshift dependent. Nevertheless we proffer the advice to use low- z data from the extensive and growing HST archives to realistically simulate the recovery of high- z $\text{Ly}\alpha$ spectral profiles in large samples.

Interestingly, the same trend in the width and offset of the red peak is observed in these higher- z systems, as discussed for $z = 0$ galaxies in Section 4.1. The normalized profiles of Figure 7 (lower left) both show the lower- $W_{\text{Ly}\alpha}$ galaxies to have both broader and less shifted red profiles; same is shown quantitatively in the right panel of Figure 6. Hashimoto et al. (2015) show the red-peak velocity shift to be much higher in LBGs than in LAEs using optical line emission such as $\text{H}\alpha$ and $[\text{O III}]$, and similar effects are probably at work here. They attributed this effect to radiation transfer effects where the LBG column density is higher, using RT modeling in spherical shells. Cassata et al. (2020) also show similar effects using the $[\text{C II}] 158 \mu\text{m}$ line: they show weak correlations of $\text{Ly}\alpha$ redshift with UV magnitude, stellar mass and SFR. These go in the direction that would support the hypothesis that mass drives the trend, but none of Cassata et al’s trends reach statistical significance, possibly because of dynamic range.

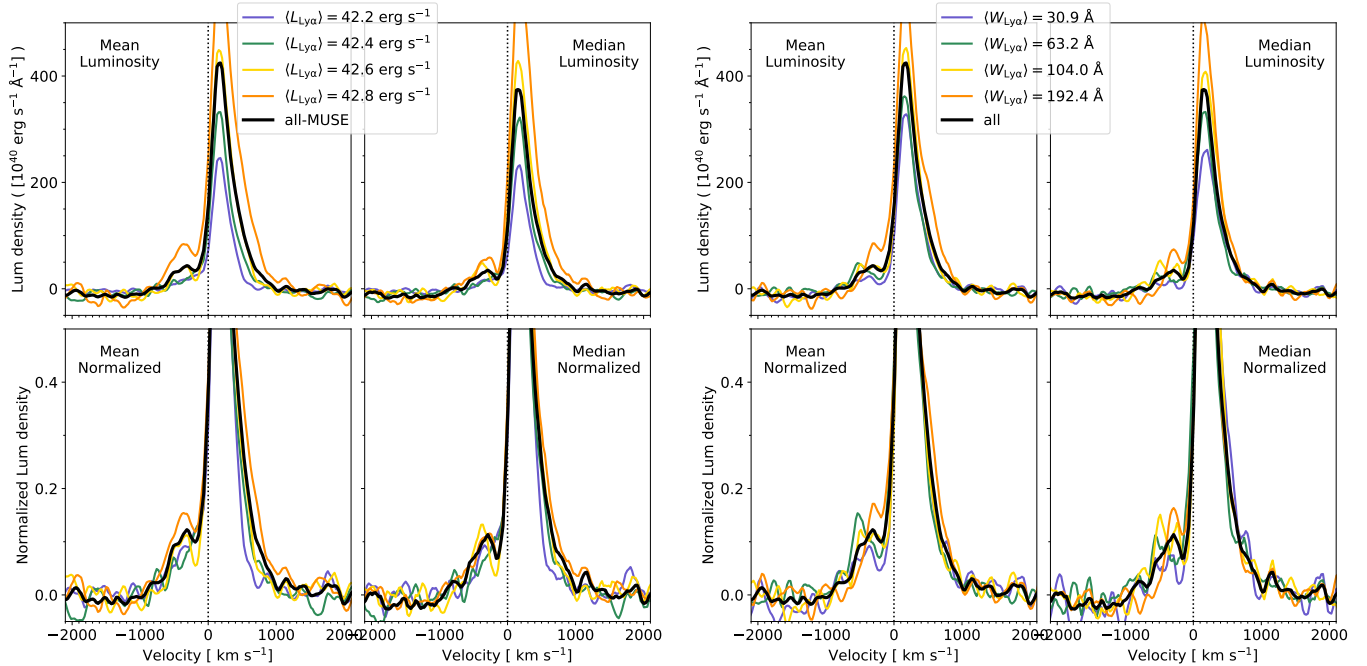


Figure 7. Same as Figure 4, but for the MUSE-WIDE sample, selecting only galaxies at $2.9 < z < 4$.

4.3. Comparison of matched samples

The COS sample from low- z is needed for an estimation of the intrinsic Ly α line profile. However, to produce such an intrinsic, IGM-free template for the high- z galaxies, we would ideally match the samples in their SFRs, masses, compactness, dust optical depths, ionizing intensities, etc. Such sample matching is far in the future and the huge majority of this information is unavailable at $z > 2.9$; obtaining it will require extensive surveys with the James Webb Space Telescope (JWST). We instead make the most basic compromise, and take only COS galaxies that overlap with the MUSE sample in the two key observables, of $L_{Ly\alpha}$ and $W_{Ly\alpha}$. The distribution of these quantities is shown in Figure 3, where the full COS sample extends to 30 times lower luminosities than the faintest MUSE-WIDE system. This is certainly to be expected when contrasting distant Ly α -selected galaxies with nearby UV-selected systems.

We impose a cut in the Ly α luminosities at 10^{42} erg s $^{-1}$, as shown by the dashed line in Figure 3. We do not aim to accurately reproduce the distributions in $W_{Ly\alpha}$ and $L_{Ly\alpha}$, but note a number of similarities. Firstly the upper envelope of the luminosity histogram is well-matched between the samples. In the $W_{Ly\alpha}$ histograms, the MUSE-WIDE survey is skewed towards somewhat higher values, with a median $W_{Ly\alpha}$ of 78 Å compared with 61 Å for the low- z sample. The Ly α blue/red flux ratio depends strongly upon $W_{Ly\alpha}$, and increases towards higher EWs as also shown in Fig-

ure 5, and this effect could introduce a bias in the direction that high- z galaxies have larger intrinsic blue/red ratios. While we do not see the same behavior in the high- z galaxies directly, we showed this to result from the stochastic IGM absorption in Section 4.2. On the other hand, the median EWs of the two samples remains close (much smaller than the interquartile range), and while acknowledging the EW difference could introduce a bias we expect it to be a minor one.

We finally note that the COS aperture ($1''.25$) samples only a projected distance of 5 kpc at $z = 0.25$, and should part of the line profile be built from extended emission then that would obviously not be captured by the low- z observation. Indeed Leclercq et al. (2020) do find differences in the velocity centroids of Ly α profiles extracted from the core and halo regions, with the implication that asymmetric profiles are built from differences between the core and halo (see also Erb et al. 2018). However we note that these conclusions from the deep MUSE data were drawn from a sub-sample in which the halo flux fraction was high by construction, skewing the interpretations in the direction of the more luminous and extended LAEs.

In the coming Section on redshift evolution, we use the COS sample to estimate the intrinsic and absorbed Ly α line profile from high- z . From now on, however, we take only low- z galaxies from the luminosity matched sub-sample ($N = 44$).

5. THE CO-EVOLUTION OF LYMAN ALPHA PROFILES AND THE INTERGALACTIC MEDIUM

In this Section we present our main results concerning the evolution of the Ly α emission line with redshift and how we can explain this in terms of the co-evolution of galaxies and the IGM.

5.1. *The Redshift Evolution of the Ly α Profile*

We now proceed to study the cosmic evolution of the Ly α profile using differential stacking comparisons, similar to those already shown. We bin the sample in redshift into five sub-samples, and show the results in Figure 8 with sample medians and half-quartile ranges shown in the caption. The high- z galaxies from the MUSE-WIDE survey are always shown in color, and the $z \approx 0.25$ sample, with no IGM, in black. At each redshift we resample the galaxy bin using bootstrap techniques. We randomly re-draw a sample of the same size and recompute the mean and median; iterating this over 1000 realizations we compute the variations of each stacked subsample about the true mean and median. For mean profiles we show the central 68th percentiles, and for the median profiles we show the interquartile range.

Several effects are clear from Figure 8. Among the most obvious, visible in the upper two panels there is a trend among the MUSE wide galaxies to become more luminous with increasing z . This is the well-known Malmquist (1922) bias, that manifests as the most luminous systems being preferentially detected. In this instance it results from the luminosity distance increasing with $(1+z)$ faster than the sensitivity of MUSE decays with $(1+z) \times \lambda_{\text{Ly}\alpha}$: even though the Ly α luminosity function is close to constant across this redshift range (e.g. Herenz et al. 2019), there is an upwards evolution of the sample luminosities because only the most luminous subset of the respective galaxy population is detected at highest redshifts.

Blue wings are visible in the profiles. This is most abundantly clear in the COS profiles from low- z , but sub-dominant blue wings are visible in the unnormalized profiles (upper). However their intensity evolution goes in the opposite direction from the evolution in the red peaks: the highest intensity blue peaks are found among the $z \approx 3-4$ subsamples, and the $L_{\text{blue}}/L_{\text{red}}$ ratios decrease with z . This is more noticeable when we normalize the profiles, which we show in the lower two panels. Here we zoom in to visualize the blue peaks: attending mainly to the median stack (lower right) the $z \approx 3-3.5$ sub stacks show normalized intensity of 10 %, which drops further to about 5 % by $z \approx 4$ and almost to zero at $z = 4.5$ and up.

In light of the Malmquist bias discussed above, a natural question becomes whether this evolution in the line profiles may result from selection effects or evolution with luminosity. This phenomenon is seen within the IGM-free COS sample (Figure 4) but not in the MUSE sample (Figure 7), and we showed with simulations (Section 4.2) that it would be impossible to detect for the given sample size and spectral quality even at $z = 3-4$. Importantly, the median luminosity evolution due to the Malmquist bias is only a factor of 2 between $z = 3$ and 5.5, which is significantly smaller than the difference between the bin median in Figure 4 where the trend is seen. We conclude that the blue peak evolution presented in Figure 8 is not attributable to selection effects of this kind.

The COS spectrum from $z \approx 0.25$ shows a $L_{\text{blue}}/L_{\text{red}}$ ratio of ≈ 16 % in the median stack, and higher still in the mean. Mean stacks, however, will always be dominated by the more luminous systems at a given velocity, and result in line profiles that are on average less representative of a given galaxy. We observe a reduction in the normalized blue peak intensity of about ≈ 60 % to $z = 3$; from a simple by-eye analysis we would estimate the an IGM opacity of $\tau_{\text{IGM}}^{1205} \approx 0.45$ from Figure 8. In the coming Section we perform a more detailed study of this.

5.2. *The Impact of the IGM*

The COS spectra are not susceptible to intergalactic Ly α absorption: the IGM optical depth at $\lambda = 1200 - 1210 \text{ \AA}$ is $\tau_{\text{IGM}}^{1205} \lesssim 10^{-6}$. Thus if the Ly α line profile observed in the COS sample is representative of the profile emergent from the CGM at redshifts beyond 3, this empirical spectrum will serve as a template. We restate that we selected the low- z sample to match the observables of the MUSE-WIDE sample in both Ly α luminosity and EW (Figure 3), which argues in favor of this utilization.

We present our finding concerning the redshift evolution of the Ly α profiles, together with simulations of the evolving IGM opacity, in Figure 9. Each column shows data and simulations for a different redshift bin, and is headed with the following text information: redshift, $W_{\text{Ly}\alpha}$, $L_{\text{Ly}\alpha}$, the number of galaxies in the bin, τ_{IGM}^{1205} from simulations, and the $L_{\text{blue}}/L_{\text{red}}$ ratio from the MUSE-WIDE stacks. The left column shows a number of results concerning the lowest redshift subset, centered at $z = 3.18$. The total Ly α profile from the stack of 46 galaxies is shown in the top row (same as red spectrum in Figure 8), and at this redshift the blue wing is very clear at low intensities, and is visible out to blueshifted velocities of 700 km s^{-1} . The median

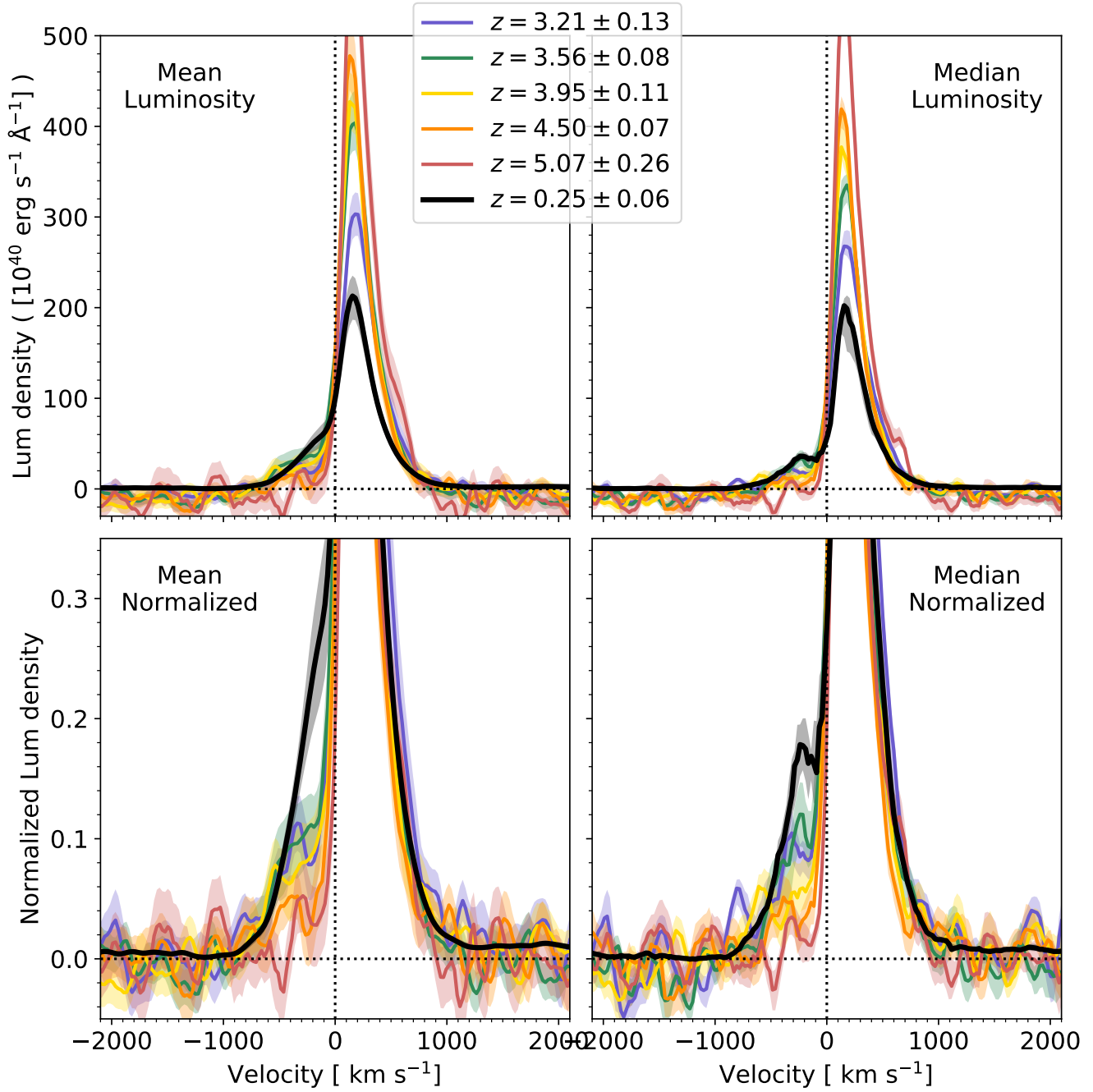


Figure 8. The evolution of the Ly α profile with redshift. The individual panels are the same as in Figures 4 and 7, but the sample is now binned by redshift; each bin includes 45 or 46 galaxies. The MUSE-WIDE sub-samples are shown in colors and the redshifts are displayed in the caption. The low- z sample observed with HST is shown in black. Error regions are shaded, and represent the interquartile range estimated from bootstrap resampling. The evolution of the blue wing, decreasing with increasing z , is obvious.

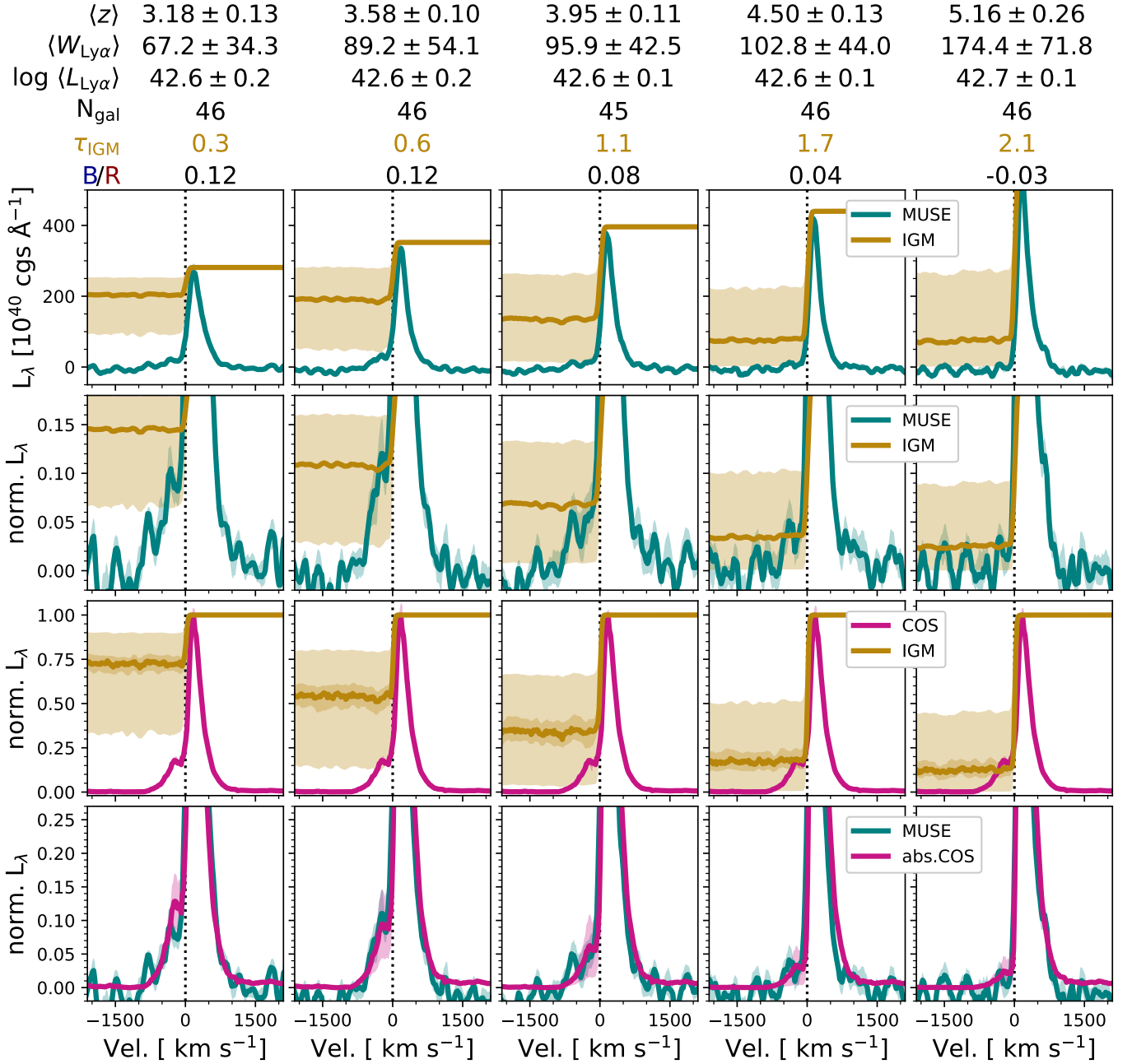


Figure 9. Simulating IGM absorption of LAEs at various redshifts. Each column shows a different redshift bin: the median z , $W_{\text{Ly}\alpha}$, $L_{\text{Ly}\alpha}$ are listed above, together with the half-quartile range of each quantity, and the number of galaxies in each bin. The top rows show the median stack of the Ly α luminosity density in absolute units ($\text{erg s}^{-1} \text{\AA}^{-1}$) in green, with the median IGM absorption overlaid, scaled so that 1 matches the red peak of the Ly α . Shaded regions represent the interquartile range. The second row shows the same Ly α profiles normalized to an intensity of 1 at the peak, and zoomed in around the wings of the line: IGM is again shown on arbitrary scale of $0.15\times$. The third row shows the stacked spectrum of the $z \approx 0$ sample in pink, always normalized to a peak intensity of 1 (same in every panel). The IGM absorption is again shown in each case, now scaled to the absolute throughput. The average optical depth, τ_{IGM}^{1205} , is computed in the $\lambda_{\text{rest}} = 1200 - 1210 \text{ \AA}$ range, and is shown at the top of each column. The lowest row shows the profile of the COS spectrum, absorbed by the IGM for each redshift bin, together with the stacked observed MUSE spectra for the same redshift. The overlap between the two lines is often striking.

IGM absorption is shown in throughput (I/I_0) in various rows for illustration: in the third row it is given in throughput on an absolute scale, and is about 0.75 on average ($\tau_{\text{IGM}}^{1205} = 0.3$), as stated in the Figure heading. This is sufficient to observably modify the shape of the Ly α profile, and suppress the blue wing, but importantly this IGM is far from thick enough to absorb all the blue-side Ly α . In the lowest panel we show the COS spectrum from $z \approx 0.25$ with the $z = 3.18$ IGM applied (pink line) overlaid upon the stacked MUSE-WIDE spectrum from the same redshift. The agreement in the average flux in the blue wing is striking. The normalized flux goes to zero in the blue wing at velocity offsets of $\lesssim -700 \text{ km s}^{-1}$ in both spectra; immediately bluewards of line-center they differ by $\approx 20\%$ in normalized intensity, with the simulated absorption from the IGM marginally over-predicting the observation from $z \sim 3$.

It is possible that this slight deficit in Ly α flux at $\Delta v \gtrsim -300 \text{ km s}^{-1}$ is due to enhanced absorption from structure/galaxies adjacent to the target LAEs. The IGM simulations follow the prescription of Inoue et al. (2014), which is constructed using the observed distribution of H I-absorbing systems identified along the sightlines to luminous quasars. Each absorber is drawn at random from a probability distribution function, and is therefore independent of all other absorbing systems and the target galaxy itself; it neglects the galaxy-galaxy spatial correlation and the fact that these LAEs should occupy somewhat over-dense regions which will enhance the absorption within the volume bound from the Hubble expansion by gravity. Precisely this has been addressed in various numerical methods (Santos 2004; Dijkstra et al. 2007; Mesinger & Furlanetto 2008; Iliev et al. 2008; Laursen et al. 2011; Gronke et al. 2020), who have all used cosmological hydrodynamical simulations to assess the distribution and velocity field of material within 10 Mpc of galaxies. In fact, such simulations have already been used to correct the Ly α EW in spectroscopic studies of high- z galaxies (Pahl et al. 2020). While the precise results will depend somewhat upon the details of the simulation and mass ranges probed by the observation, the broad picture is clear: at $z \approx 3 - 3.5$ sample there is a sharp excess of Ly α absorption at velocities ≈ -50 to -100 km s^{-1} from line-center that increases the Ly α absorption by a factor of two to three times. This excess of absorption returns to the baseline value (random absorption systems) at velocity offsets exceeding $\approx 300 \text{ km s}^{-1}$, and it seems entirely plausible that this phenomenon could explain the deficit of blue-side flux close to line-center at the lower redshift end of the MUSE sample. However, we note while this excess absorption due to circumgalactic material is visible for all

halo masses at $z \gtrsim 3$ in the simulations, it is not required to explain the stacked spectra studied here.

We now proceed to examine the next redshift bin, centered at $z = 3.55$. The MUSE-WIDE galaxies at this redshift completely match with those of the previous bin in $L_{\text{Ly}\alpha}$; and the median EWs are consistent within 8 \AA ($\approx 25\%$ the half-quartile range; values quoted above the figure rows). By this redshift the IGM optical depth has increased by a factor of two (0.3 to 0.6) and provides significantly more absorption on average. When we use this IGM absorption profile to artificially attenuate the COS spectrum we bring the COS and MUSE blue components into tight agreement at all velocities between -1000 and 0 km s^{-1} . Indeed the absorbed COS spectrum completely overlies the MUSE stack, with no need for excess absorption at any velocity; it is difficult to tell which stack is which.

The IGM opacity increases systematically, with τ_{IGM}^{1205} going from 1.1, to 1.8, to 2.3 at redshifts $z = 3.9, 4.5,$ and 5.4 , respectively. If we take the typical $L_{\text{blue}}/L_{\text{red}}$ ratios observed at low- z as representative (~ 0.35 ; Figure 5), then we would expect the blue bumps to reach approximately 0.1, 0.06, and 0.03 in the absorbed spectra that are normalized to the red peak. This is precisely what is shown in columns 3, 4, and 5 of Figure 9: probable blue bumps remain but if real their significance is low, and their normalized intensity is reduced to the level of a few per-cent. At none of these higher redshifts do we need an additional component of absorption at low blueshifted velocities, that we attributed to structure near to the galaxies or cosmic infall (e.g. Dijkstra et al. 2007; Laursen et al. 2011).

6. DISCUSSION

6.1. Radiation Transfer Simulations in Realistic Environments

In recent years a number of theoretical efforts have been devoted to predicting the Ly α output of galaxies from RT models, using two complementary approaches. Researchers have used idealized model galaxies described by a number of single parameters (gas column density, outflow velocity, etc) to examine how Ly α profiles vary with these basic properties (e.g. Verhamme et al. 2006; Schaerer et al. 2011; Gronke & Dijkstra 2016): the main criticism leveled at these studies is that realistic galaxies are not well described by such simplistic models, so the community instead turns to simulated galaxies to produce the manifold for RT simulations (e.g. Tasitsiomi 2006; Laursen & Sommer-Larsen 2007; Faucher-Giguère et al. 2010; Zheng et al. 2010; Barnes et al. 2011; Trebitsch et al. 2016; Smith et al. 2019). These models are not without criticism ei-

ther, and are often cited as having insufficient spatial resolution, particularly at CGM scales, to capture the representative geometry for the RT. RT in these settings almost invariably over-produces Ly α emission on the blue side of line center, at a level that is only very rarely found by observation. The proponents frequently appeal to intergalactic absorption to remove the blue component, but our results show that this appeal is unlikely to be realistic. The uncorrelated Ly α absorbing systems do not reach sufficient opacity to universally suppress the blue emission seen in starburst galaxies, and we find no need within this large dataset for an excess opacity near galaxies. However, we also note that LAEs such as these do reside in lower-mass halos, and there still may be room for the effect to be more prominent on sightlines towards higher halo mass.

6.2. *Is there still space for excess opacity?*

The absence of enhanced Ly α within a few hundred kms^{-1} of the galaxies is worthy of further discussion. One explanation could be that with structure building up hierarchically over time, we need to wait until redshifts ~ 3 for significant *neutral* gas to affect the Ly α line to an extent greater than the uncorrelated cosmic average. One may speculate that the galaxies studied here are less massive than those studied in the simulations referred to above, and the amplitude of their overdensity/infall compared to the cosmic mean will be lower. However with the typical range of stellar masses in the mock galaxies being $\approx 10^7 - 10^{10} M_{\odot}$ this seems unlikely on average as LAEs of this luminosity probably have $M_{\text{stell}} \approx 10^8 - 10^9 M_{\odot}$. Alternatively, the gas may be more ionized than thought, which would imply the simulated opacity is overestimated. This might be due to a lower clumping factor of cold, neutral material (e.g., because of a lack of spatial resolution; van de Voort et al. 2019; Hummels et al. 2019) or additional ionization sources. We may point towards photoionization of low-mass companion structures by the enhanced UV background close to early galaxies, where the excess UV results from numerous galaxies that are too faint to be detected. Such galaxies may, however, be visible in the ultra-deep MUSE pointings (e.g. Bacon et al. 2017).

We also question whether this absence of excess blue-side absorption could be the result of a conspiracy of parameters, where the intrinsic $L_{\text{blue}}/L_{\text{red}}$ does increase with z , but is suppressed by absorption on small scales. Indeed the Malmquist bias results in an upwards evolution of $L_{\text{Ly}\alpha}$ with z (Figure 8, upper) which may be expected to increase the intrinsic $L_{\text{blue}}/L_{\text{red}}$ (Figures 4 and 5). However we note that the trends that are revealed in the COS sample are manifested over a dynamic range of

almost 2 dex, whereas the overall evolution introduced by the Malmquist bias is just a factor of 2 between $z = 3$ and 5.5. In fact, attending to the sample medians shown at the top of Figure 9, there is very little evolution in total (observed) $L_{\text{Ly}\alpha}$. So while cannot rule this out a conspiracy of parameters, we believe the dynamic range, coupled with the relatively small Malmquist bias, are insufficient to produce an effect of the required magnitude.

6.3. *Less blueshifted Ly α , but more Ly α overall*

We note also that this downwards evolution of the blue contribution, and clearly increasing impact of the IGM, occurs against the backdrop of an overall *increasing* Ly α output from the galaxy population. This is shown by numerous lines of evidence including a Ly α fraction among LBGs that increases significantly over the same redshift range we probe here (Stark et al. 2010; Cassata et al. 2015; De Barros et al. 2017, although see also Caruana et al. 2018), an increase in the volume-averaged Ly α escape fraction of galaxies (Hayes et al. 2011; Dijkstra & Jeeson-Daniel 2013; Konno et al. 2016; Wold et al. 2017), and the increasing agreement of the UV LFs of LAEs and LBGs (Ouchi et al. 2008). In these first papers we could only speculate about the actual influence the IGM has on the Ly α emission: because the Ly α output *increases* with z , we concluded the IGM could not act to strongly suppress Ly α . The new evidence presented here shows that this is not the case, and if the COS-measured $L_{\text{blue}}/L_{\text{red}}$ of ≈ 0.35 continues to hold at high- z (or even grow), then the IGM removes an additional quarter of the total Ly α (integrated over the whole line) at $z = 5.5$ compared to 3. The implication is that the Ly α emitted from galaxies must increase by a corresponding amount over the same redshift range in order to counteract this effect. Such excess emission may be attributed to the decreasing dust content, stellar metallicity, or average age of galaxies with redshift, implying they must evolve even faster than previously claimed (e.g. Hayes et al. 2011).

7. OUTLOOK AND LIMITATIONS

In Section 3 we showed that there is real and strong evolution in the relative contribution of the blue wing of the Ly α emission with redshift, and in Section 5.2 that we are able to fully reproduce this with IGM absorption. The main assumptions were that the intrinsic Ly α spectrum is invariant with redshift and can be described by the profile of low- z sample observed with HST/COS, and that the IGM is spatially uncorrelated and does not require an enhancement from companion galaxies/proximate Lyman limit systems. Furthermore the remarkable agreement between the Ly α profiles

at all z , supports the utility of our improved heuristic z_{sys} estimation from analysis of the Ly α line profile (A. Runholm et al 2020b, in prep), despite an evolution in the IGM opacity (τ_{IGM}^{1205}) of more than two optical depths. This naturally raises the question of to what extent the observed evolution of the Ly α profile can be used to infer the IGM opacity at even higher redshifts, and into the epoch reionization (EoR).

As mentioned in Section 1 strong blueshifted emission peaks have also been found at $z = 5.8 - 6.6$. Some prime examples include Aerith B at $z = 5.8$ (Bosman et al. 2019), NEPLA4 at $z = 6.5$ (Songaila et al. 2018) and COLA1 at $z = 6.6$ (Hu et al. 2016; Matthee et al. 2018), which all show spectacular Ly α profiles, with dominant red lines but inarguable blue peaks. Songaila et al. (2018) suggest that such spectral features may be present in the profiles of less luminous galaxies in significant numbers of up to 1/3. This is quite unexpected in light of the results shown in Figures 8 and 9, but two key points must be born in mind when co-interpreting the datasets. Firstly our analysis is based upon stacking which acts as a lossy compression that removes all information concerning the dispersion within the sample. If blue bumps are present at $z > 5$ in the galaxies from the Urrutia et al. (2019) data release, as a significant minority, they will not be represented in the median stacking (right columns) and will be hard to detect in the averaging. Secondly the $z > 5.7$ blue-bump objects mentioned above are all significantly more luminous than MUSE-WIDE galaxies: typical $\log(L_{\text{Ly}\alpha}/(\text{erg s}^{-1}))$ is 43.5, while our $z \approx 5.2$ subsample has a median luminosity that is 0.8 dex lower.

As we are likely unable to identify blue bumps in the MUSE-WIDE data, this makes comparison to the more luminous systems difficult. For a fixed Ly α escape fraction, the ‘ordinary’ systems studied here would themselves be almost ten times less ionizing than the luminous blue-bump galaxies. Nevertheless, the overwhelming majority of the ionizing photons required to ionize a bubble with radius at least 1 Mpc come from sources other than the galaxy itself, even for more luminous galaxies (Bagley et al. 2017), we should be wary of over-interpreting spectra of single galaxies. Even in the case of very large H II regions, the presence/absence of blue peaks/wings may have more to do with the galaxy’s position along the line-of-sight with respect to the bubble edges, and the details of its ISM, than with the IGM state.

One limitation of our study is that our galaxies are Ly α -selected. At the higher ends of mid- z ($z \sim 4 - 5.5$) this may remain a representative sample of the galaxy population: the average Ly α output of galaxies contin-

ually increases (Stark et al. 2010; Hayes et al. 2011). However all these Ly α -quantities begin to drop after $z \sim 6.5$ (Schenker et al. 2012), which raises doubts about the utility of LAE-based probes at higher redshifts. At these redshifts the Ly α -based studies may provide representative statistics about the geometry of H II bubbles, but not about the regions between, which must still be probed with (most likely) UV-selected/Lyman break galaxies.

In the coming years, Subaru Prime Focus Spectrograph (PFS) will embark upon very large area Ly α surveys (14 deg² under the Subaru Strategic Program) targeting UV-selected galaxies over what is likely to be the complete range of bubble distributions in the EoR. PFS can target Ly α at $\lesssim 6.3$ at $R \approx 5000$ with the mid-resolution red spectrograph, and at $\gtrsim 6.7$ at $R \approx 4300$ with the NIR spectrograph; the gap between the two redshifts can be filled by the low-resolution red spectrograph at $R \approx 3000$, which is comparable to MUSE at these redshifts. An obvious study therefore becomes the behavior of the Ly α profile as a function of local galaxy environment, in which the blue contribution to the total Ly α can be used to constrain the dispersion on τ_{IGM} at fixed redshift. This paper, and Figure 9 in particular, shows that this goal can be reached at the expected resolving powers of PFS. Indeed the same goal cannot efficiently be reached the VLT/MUSE because of the small survey volume at the highest redshifts.

The natural drawback of this fiber-fed approach, of course, is that it demands photometric pre-selection, and will not have the possibility to identify new LAEs within its own observation. The SSP will target LBGs and LAEs from SSP imaging surveys GOLDRUSH and SILVERRUSH, and as a consequence the Ly α -emitter components will be limited to the narrowband depths, which currently fall around $\log(L_{\text{Ly}\alpha}/(\text{erg s}^{-1})) = 43.0$ for SILVERRUSH (Konno et al. 2018). Thus the survey will deliver huge numbers of spectra with luminosities close to those of COLA1 and NEPLA4, and LBGs from GOLDRUSH that are more massive still, it remains unclear how well the survey will sample the mass range of more ‘normal’ star-forming LAEs at similar redshift. Thus the observational necessity remains for deep IFU studies with instruments like MUSE, that deliver 100% spectroscopic completeness with the contrast and depth that can only be provided by spectroscopic surveys.

8. SUMMARY AND CONCLUSIONS

We have undertaken an extensive study of the Ly α emission line profile from star forming galaxies at various cosmic epochs, using some of the largest samples of available spectra obtained with HST/COS at low- z and

VLT/MUSE at $z = 2.9$ to 6.6 . Our main findings can be summarized as:

- We see distinct and predictable variations in the shape of the Ly α profile in the low- z sample. The blue peak gets stronger with increasing $W_{\text{Ly}\alpha}$. We believe this trend results from atomic gas column being the dominant factor in regulating Ly α output, and as the galaxies almost certainly have outflows the blue peak is more significantly suppressed than the red.
- This trend is not observed within the MUSE sample at $z = 2.9 - 4$ ($N = 74$ galaxies). Using Monte Carlo bootstrap simulations of the IGM opacity and applying them to the low- z sample, we show that the stochastic nature of IGM opacity to Ly α is entirely sufficient to remove trends of this amplitude.
- We find the red component of the Ly α profile becomes broader and increasingly redshifted at lower Ly α equivalent widths. We attribute these effects to the covering of atomic material. More scattering increases the absorption of Ly α and preferentially in the blue wing while, at the same time, the larger column density requires longer frequency excursions to escape, resulting in broader, more redshifted lines.
- Using basic Ly α observables of $L_{\text{Ly}\alpha}$ and $W_{\text{Ly}\alpha}$, we identify a Ly α -matched sample of galaxies at $z \lesssim 0.4$. The COS sample shows a significantly

higher average blue peak than the $z \gtrsim 3$ galaxies, with roughly twice the intensity in the blue bump. The blue-bump amplitude of the high- z sample decreases systematically from $z = 3$ and upwards, becoming undetectable by $z \approx 5.5$.

- The evolution of the average observed Ly α profile with redshift is very well described by adopting the average profile from low- z and absorbing it with the current best estimates for the IGM opacity as a function of redshift. This IGM prescription does not account for line-of-sight correlation in the absorbers, and assumes they are random in redshift – we do not find evidence for additional absorption of Ly α resulting from small scale structure and peculiar motions/infall in adjacent to galaxies.

ACKNOWLEDGEMENTS

We are grateful to the core members of the MUSE-WIDE team – Lutz Wisotzki, Tanya Urrutia, and E. Christian Herenz – for making the extracted spectra available and enabling this project. We thank the same MUSE-WIDE team, and also Peter Laursen, for useful discussions. M.H. acknowledges the support of the Swedish Research Council, Vetenskapsrådet and the Swedish National Space Agency (SNSA), and is Fellow of the Knut and Alice Wallenberg Foundation. M.G. was supported by NASA through the NASA Hubble Fellowship grant HST-HF2-51409 and acknowledges support from HST grants HST-GO-15643.017-A, HST-AR-15039.003-A, and XSEDE grant TG-AST180036.

REFERENCES

- Adams, T. F. 1972, ApJ, 174, 439, doi: [10.1086/151503](https://doi.org/10.1086/151503)
- Bacon, R., Accardo, M., Adjali, L., et al. 2010, in Society of Photo-Optical Instrumentation Engineers (SPIE) Conference Series, Vol. 7735, Proc. SPIE, 773508
- Bacon, R., Vernet, J., Borisova, E., et al. 2014, The Messenger, 157, 13
- Bacon, R., Conseil, S., Mary, D., et al. 2017, A&A, 608, A1, doi: [10.1051/0004-6361/201730833](https://doi.org/10.1051/0004-6361/201730833)
- Bagley, M. B., Scarlata, C., Henry, A., et al. 2017, ApJ, 837, 11, doi: [10.3847/1538-4357/837/1/11](https://doi.org/10.3847/1538-4357/837/1/11)
- Barnes, L. A., Haehnelt, M. G., Tescari, E., & Viel, M. 2011, MNRAS, 416, 1723, doi: [10.1111/j.1365-2966.2011.18789.x](https://doi.org/10.1111/j.1365-2966.2011.18789.x)
- Bosman, S. E. I., Kakiichi, K., Meyer, R. A., et al. 2019, arXiv e-prints, arXiv:1912.11486. <https://arxiv.org/abs/1912.11486>
- Caruana, J., Wisotzki, L., Herenz, E. C., et al. 2018, MNRAS, 473, 30, doi: [10.1093/mnras/stx2307](https://doi.org/10.1093/mnras/stx2307)
- Cassata, P., Tasca, L. A. M., Le Fèvre, O., et al. 2015, A&A, 573, A24, doi: [10.1051/0004-6361/201423824](https://doi.org/10.1051/0004-6361/201423824)
- Cassata, P., Morselli, L., Faisst, A., et al. 2020, arXiv e-prints, arXiv:2002.00967. <https://arxiv.org/abs/2002.00967>
- Cowie, L. L., Barger, A. J., & Hu, E. M. 2011, ApJ, 738, 136, doi: [10.1088/0004-637X/738/2/136](https://doi.org/10.1088/0004-637X/738/2/136)
- Curtis-Lake, E., McLure, R. J., Pearce, H. J., et al. 2012, MNRAS, 422, 1425, doi: [10.1111/j.1365-2966.2012.20720.x](https://doi.org/10.1111/j.1365-2966.2012.20720.x)
- De Barros, S., Pentericci, L., Vanzella, E., et al. 2017, A&A, 608, A123, doi: [10.1051/0004-6361/201731476](https://doi.org/10.1051/0004-6361/201731476)
- Dijkstra, M. 2014, PASA, 31, e040, doi: [10.1017/pasa.2014.33](https://doi.org/10.1017/pasa.2014.33)

- Dijkstra, M., & Jeeson-Daniel, A. 2013, MNRAS, 435, 3333, doi: [10.1093/mnras/stt1520](https://doi.org/10.1093/mnras/stt1520)
- Dijkstra, M., Lidz, A., & Wyithe, J. S. B. 2007, MNRAS, 377, 1175, doi: [10.1111/j.1365-2966.2007.11666.x](https://doi.org/10.1111/j.1365-2966.2007.11666.x)
- Erb, D. K. 2015, Nature, 523, 169, doi: [10.1038/nature14454](https://doi.org/10.1038/nature14454)
- Erb, D. K., Pettini, M., Steidel, C. C., et al. 2016, ApJ, 830, 52, doi: [10.3847/0004-637X/830/1/52](https://doi.org/10.3847/0004-637X/830/1/52)
- Erb, D. K., Steidel, C. C., & Chen, Y. 2018, ApJL, 862, L10, doi: [10.3847/2041-8213/aacff6](https://doi.org/10.3847/2041-8213/aacff6)
- Erb, D. K., Steidel, C. C., Trainor, R. F., et al. 2014, ApJ, 795, 33, doi: [10.1088/0004-637X/795/1/33](https://doi.org/10.1088/0004-637X/795/1/33)
- Faucher-Giguère, C.-A., Kereš, D., Dijkstra, M., Hernquist, L., & Zaldarriaga, M. 2010, ApJ, 725, 633, doi: [10.1088/0004-637X/725/1/633](https://doi.org/10.1088/0004-637X/725/1/633)
- Green, J. C., Froning, C. S., Osterman, S., et al. 2012, ApJ, 744, 60, doi: [10.1088/0004-637X/744/1/60](https://doi.org/10.1088/0004-637X/744/1/60)
- Gronke, M., & Dijkstra, M. 2016, ApJ, 826, 14, doi: [10.3847/0004-637X/826/1/14](https://doi.org/10.3847/0004-637X/826/1/14)
- Gronke, M., Ocvirk, P., Mason, C., et al. 2020, arXiv e-prints, arXiv:2004.14496. <https://arxiv.org/abs/2004.14496>
- Guo, Y., Ferguson, H. C., Giallisco, M., et al. 2013, ApJS, 207, 24, doi: [10.1088/0067-0049/207/2/24](https://doi.org/10.1088/0067-0049/207/2/24)
- Hashimoto, T., Verhamme, A., Ouchi, M., et al. 2015, ApJ, 812, 157, doi: [10.1088/0004-637X/812/2/157](https://doi.org/10.1088/0004-637X/812/2/157)
- Hashimoto, T., Laporte, N., Mawatari, K., et al. 2018, Nature, 557, 392, doi: [10.1038/s41586-018-0117-z](https://doi.org/10.1038/s41586-018-0117-z)
- Hayes, M. 2015, PASA, 32, 27, doi: [10.1017/pasa.2015.25](https://doi.org/10.1017/pasa.2015.25)
- Hayes, M., Schaerer, D., Östlin, G., et al. 2011, ApJ, 730, 8, doi: [10.1088/0004-637X/730/1/8](https://doi.org/10.1088/0004-637X/730/1/8)
- Heckman, T. M., Alexandroff, R. M., Borthakur, S., Overzier, R., & Leitherer, C. 2015, ApJ, 809, 147, doi: [10.1088/0004-637X/809/2/147](https://doi.org/10.1088/0004-637X/809/2/147)
- Heckman, T. M., Borthakur, S., Overzier, R., et al. 2011, ApJ, 730, 5, doi: [10.1088/0004-637X/730/1/5](https://doi.org/10.1088/0004-637X/730/1/5)
- Henry, A., Scarlata, C., Martin, C. L., & Erb, D. 2015, ApJ, 809, 19, doi: [10.1088/0004-637X/809/1/19](https://doi.org/10.1088/0004-637X/809/1/19)
- Herenz, E. C., Urrutia, T., Wisotzki, L., et al. 2017, A&A, 606, A12, doi: [10.1051/0004-6361/201731055](https://doi.org/10.1051/0004-6361/201731055)
- Herenz, E. C., Wisotzki, L., Saust, R., et al. 2019, A&A, 621, A107, doi: [10.1051/0004-6361/201834164](https://doi.org/10.1051/0004-6361/201834164)
- Hu, E. M., Cowie, L. L., Songaila, A., et al. 2016, ApJL, 825, L7, doi: [10.3847/2041-8205/825/1/L7](https://doi.org/10.3847/2041-8205/825/1/L7)
- Hummels, C. B., Smith, B. D., Hopkins, P. F., et al. 2019, ApJ, 882, 156, doi: [10.3847/1538-4357/ab378f](https://doi.org/10.3847/1538-4357/ab378f)
- Hummer, D. G., & Rybicki, G. 1971, ARA&A, 9, 237, doi: [10.1146/annurev.aa.09.090171.001321](https://doi.org/10.1146/annurev.aa.09.090171.001321)
- Iliev, I. T., Shapiro, P. R., McDonald, P., Mellema, G., & Pen, U.-L. 2008, MNRAS, 391, 63, doi: [10.1111/j.1365-2966.2008.13879.x](https://doi.org/10.1111/j.1365-2966.2008.13879.x)
- Inoue, A. K., Shimizu, I., Iwata, I., & Tanaka, M. 2014, MNRAS, 442, 1805, doi: [10.1093/mnras/stu936](https://doi.org/10.1093/mnras/stu936)
- Izotov, Y. I., Schaerer, D., Thuan, T. X., et al. 2016, MNRAS, 461, 3683, doi: [10.1093/mnras/stw1205](https://doi.org/10.1093/mnras/stw1205)
- Izotov, Y. I., Schaerer, D., Worseck, G., et al. 2020, MNRAS, 491, 468, doi: [10.1093/mnras/stz3041](https://doi.org/10.1093/mnras/stz3041)
- Izotov, Y. I., Worseck, G., Schaerer, D., et al. 2018, MNRAS, 478, 4851, doi: [10.1093/mnras/sty1378](https://doi.org/10.1093/mnras/sty1378)
- Jaskot, A. E., Dowd, T., Oey, M. S., Scarlata, C., & McKinney, J. 2019, ApJ, 885, 96, doi: [10.3847/1538-4357/ab3d3b](https://doi.org/10.3847/1538-4357/ab3d3b)
- Jaskot, A. E., & Oey, M. S. 2014, ApJL, 791, L19, doi: [10.1088/2041-8205/791/2/L19](https://doi.org/10.1088/2041-8205/791/2/L19)
- Jaskot, A. E., Oey, M. S., Scarlata, C., & Dowd, T. 2017, ApJL, 851, L9, doi: [10.3847/2041-8213/aa9d83](https://doi.org/10.3847/2041-8213/aa9d83)
- Kakiichi, K., & Gronke, M. 2019, arXiv e-prints, arXiv:1905.02480. <https://arxiv.org/abs/1905.02480>
- Kashikawa, N., Shimasaku, K., Malkan, M. A., et al. 2006, ApJ, 648, 7, doi: [10.1086/504966](https://doi.org/10.1086/504966)
- Kimm, T., Blaizot, J., Garel, T., et al. 2019, MNRAS, 486, 2215, doi: [10.1093/mnras/stz989](https://doi.org/10.1093/mnras/stz989)
- Konno, A., Ouchi, M., Nakajima, K., et al. 2016, ApJ, 823, 20, doi: [10.3847/0004-637X/823/1/20](https://doi.org/10.3847/0004-637X/823/1/20)
- Konno, A., Ouchi, M., Shibuya, T., et al. 2018, PASJ, 70, S16, doi: [10.1093/pasj/psx131](https://doi.org/10.1093/pasj/psx131)
- Kusakabe, H., Blaizot, J., Garel, T., et al. 2020, arXiv e-prints, arXiv:2003.12083. <https://arxiv.org/abs/2003.12083>
- Laursen, P., & Sommer-Larsen, J. 2007, ApJL, 657, L69, doi: [10.1086/513191](https://doi.org/10.1086/513191)
- Laursen, P., Sommer-Larsen, J., & Razoumov, A. O. 2011, ApJ, 728, 52, doi: [10.1088/0004-637X/728/1/52](https://doi.org/10.1088/0004-637X/728/1/52)
- Leclercq, F., Bacon, R., Verhamme, A., et al. 2020, A&A, 635, A82, doi: [10.1051/0004-6361/201937339](https://doi.org/10.1051/0004-6361/201937339)
- Malhotra, S., & Rhoads, J. E. 2004, ApJL, 617, L5, doi: [10.1086/427182](https://doi.org/10.1086/427182)
- . 2006, ApJL, 647, L95, doi: [10.1086/506983](https://doi.org/10.1086/506983)
- Malmquist, K. G. 1922, Meddelanden fran Lunds Astronomiska Observatorium Serie I, 100, 1
- Mason, C. A., & Gronke, M. 2020, arXiv e-prints, arXiv:2004.13065. <https://arxiv.org/abs/2004.13065>
- Mason, C. A., Treu, T., de Barros, S., et al. 2018, ApJL, 857, L11, doi: [10.3847/2041-8213/aabbab](https://doi.org/10.3847/2041-8213/aabbab)
- Matthee, J., Sobral, D., Gronke, M., et al. 2018, A&A, 619, A136, doi: [10.1051/0004-6361/201833528](https://doi.org/10.1051/0004-6361/201833528)
- Mesinger, A., & Furlanetto, S. R. 2008, MNRAS, 385, 1348, doi: [10.1111/j.1365-2966.2007.12836.x](https://doi.org/10.1111/j.1365-2966.2007.12836.x)
- Neufeld, D. A. 1990, ApJ, 350, 216, doi: [10.1086/168375](https://doi.org/10.1086/168375)
- Ono, Y., Ouchi, M., Mobasher, B., et al. 2012, ApJ, 744, 83, doi: [10.1088/0004-637X/744/2/83](https://doi.org/10.1088/0004-637X/744/2/83)

- Osterbrock, D. E. 1962, *ApJ*, 135, 195, doi: [10.1086/147258](https://doi.org/10.1086/147258)
- Ouchi, M., Shimasaku, K., Akiyama, M., et al. 2008, *ApJS*, 176, 301, doi: [10.1086/527673](https://doi.org/10.1086/527673)
- Pahl, A. J., Shapley, A., Faisst, A. L., et al. 2020, *MNRAS*, 493, 3194, doi: [10.1093/mnras/staa355](https://doi.org/10.1093/mnras/staa355)
- Pentericci, L., Vanzella, E., Fontana, A., et al. 2014, *ApJ*, 793, 113, doi: [10.1088/0004-637X/793/2/113](https://doi.org/10.1088/0004-637X/793/2/113)
- Rivera-Thorsen, T. E., Östlin, G., Hayes, M., & Puschig, J. 2017, *ApJ*, 837, 29, doi: [10.3847/1538-4357/aa5d0a](https://doi.org/10.3847/1538-4357/aa5d0a)
- Rivera-Thorsen, T. E., Hayes, M., Östlin, G., et al. 2015, *ApJ*, 805, 14, doi: [10.1088/0004-637X/805/1/14](https://doi.org/10.1088/0004-637X/805/1/14)
- Runnholm, A., Hayes, M., Melinder, J., et al. 2020, *ApJ*, 892, 48, doi: [10.3847/1538-4357/ab7a91](https://doi.org/10.3847/1538-4357/ab7a91)
- Rupke, D. 2018, *Galaxies*, 6, 138, doi: [10.3390/galaxies6040138](https://doi.org/10.3390/galaxies6040138)
- Santos, M. R. 2004, *MNRAS*, 349, 1137, doi: [10.1111/j.1365-2966.2004.07594.x](https://doi.org/10.1111/j.1365-2966.2004.07594.x)
- Schaerer, D., Hayes, M., Verhamme, A., & Teyssier, R. 2011, *A&A*, 531, A12, doi: [10.1051/0004-6361/201116709](https://doi.org/10.1051/0004-6361/201116709)
- Schenker, M. A., Stark, D. P., Ellis, R. S., et al. 2012, *ApJ*, 744, 179, doi: [10.1088/0004-637X/744/2/179](https://doi.org/10.1088/0004-637X/744/2/179)
- Smith, A., Ma, X., Bromm, V., et al. 2019, *MNRAS*, 484, 39, doi: [10.1093/mnras/sty3483](https://doi.org/10.1093/mnras/sty3483)
- Songaila, A., Hu, E. M., Barger, A. J., et al. 2018, *ApJ*, 859, 91, doi: [10.3847/1538-4357/aac021](https://doi.org/10.3847/1538-4357/aac021)
- Stark, D. P., Ellis, R. S., Chiu, K., Ouchi, M., & Bunker, A. 2010, *MNRAS*, 408, 1628, doi: [10.1111/j.1365-2966.2010.17227.x](https://doi.org/10.1111/j.1365-2966.2010.17227.x)
- Tasitsiomi, A. 2006, *ApJ*, 645, 792, doi: [10.1086/504460](https://doi.org/10.1086/504460)
- Trainor, R. F., Strom, A. L., Steidel, C. C., & Rudie, G. C. 2016, *ApJ*, 832, 171, doi: [10.3847/0004-637X/832/2/171](https://doi.org/10.3847/0004-637X/832/2/171)
- Trebitsch, M., Verhamme, A., Blaizot, J., & Rosdahl, J. 2016, *A&A*, 593, A122, doi: [10.1051/0004-6361/201527024](https://doi.org/10.1051/0004-6361/201527024)
- Urrutia, T., Wisotzki, L., Kerutt, J., et al. 2019, *A&A*, 624, A141, doi: [10.1051/0004-6361/201834656](https://doi.org/10.1051/0004-6361/201834656)
- van de Voort, F., Springel, V., Mandelker, N., van den Bosch, F. C., & Pakmor, R. 2019, *MNRAS*, 482, L85, doi: [10.1093/mnrasl/sly190](https://doi.org/10.1093/mnrasl/sly190)
- Veilleux, S., Maiolino, R., Bolatto, A. D., & Aalto, S. 2020, *A&A Rv*, 28, 2, doi: [10.1007/s00159-019-0121-9](https://doi.org/10.1007/s00159-019-0121-9)
- Verhamme, A., Orlitová, I., Schaerer, D., & Hayes, M. 2015, *A&A*, 578, A7, doi: [10.1051/0004-6361/201423978](https://doi.org/10.1051/0004-6361/201423978)
- Verhamme, A., Schaerer, D., & Maselli, A. 2006, *A&A*, 460, 397, doi: [10.1051/0004-6361:20065554](https://doi.org/10.1051/0004-6361:20065554)
- Wofford, A., Leitherer, C., & Salzer, J. 2013, *ApJ*, 765, 118, doi: [10.1088/0004-637X/765/2/118](https://doi.org/10.1088/0004-637X/765/2/118)
- Wold, I. G. B., Finkelstein, S. L., Barger, A. J., Cowie, L. L., & Rosenwasser, B. 2017, *ApJ*, 848, 108, doi: [10.3847/1538-4357/aa8d6b](https://doi.org/10.3847/1538-4357/aa8d6b)
- Yang, H., Malhotra, S., Gronke, M., et al. 2017, *ApJ*, 844, 171, doi: [10.3847/1538-4357/aa7d4d](https://doi.org/10.3847/1538-4357/aa7d4d)
- Zheng, Z., Cen, R., Trac, H., & Miralda-Escudé, J. 2010, *ApJ*, 716, 574, doi: [10.1088/0004-637X/716/1/574](https://doi.org/10.1088/0004-637X/716/1/574)